DESIGN OF THE PERMANENT MAGNET BEARING OF THE MAGLEV ARTIFICIAL HEART

Hiroyuki Onuma, Michiko Murakami, Toru Masuzawa
Department of Mechanical Engineering, Ibaraki University, Hitachi, Ibaraki 316-8511 JAPAN
honuma@mech.ibaraki.ac.jp, nm3438n@hcs.ibaraki.ac.jp, masuzawa@mech.ibaraki.ac.jp

ABSTRACT

We have developed a magnetically suspended centrifugal blood pump that consists of combined active and passive magnetic bearings to be used as a durable ventricular assist device. The Maglev centrifugal pump designed in this work consists of an active magnetic bearing, a permanent magnet bearing (PM bearing), a levitated impeller, and a motor stator. Two types of PM bearings were designed based on a numerical simulation performed prior to construction. Both of these PM bearings were capable of restricting the radial movement of the levitated impeller without deterioration of the axial position control performance. The maximum rotation speed for both types of pumps was 2000 rpm with pumping. The maximum amplitude in the axial direction was only 0.05 mm. The Maglev centrifugal pump designed here displayed sufficient magnetic suspension ability and pump performance to be used as a ventricular assist device.

INTRODUCTION

Magnetically suspended centrifugal blood pumps have been developed as implantable ventricular assist devices for long-term use [1-4]. The absence of contact that is typical in the Maglev pump makes for high durability, lower hemolysis properties, and anti-thrombogenesity. Axial movements and tilt of the levitated impeller are controlled with electromagnets in our system. The radial movement of the levitated impeller is restricted by a permanent magnet bearing (PM bearing) to reduce energy consumption and the required complexity of the controller. In this paper, the design concept of these PM bearings for this type of artificial heart is reported.

METHODS

Maglev centrifugal blood pump

Figure 1 shows the Maglev centrifugal blood pump. The Maglev centrifugal blood pump consists of a top stator, a rotor-impeller, and a bottom stator. The rotor-impeller is set between the top and the bottom stator. The top stator has four electro-magnetic coils to control the tilt and the axial position of the rotor-impeller. The bottom stator has twelve electro-magnetic coils to control the rotation. The radial movement of the rotor-impeller is restricted passively by using the PM bearing, which consists of two ring-shaped permanent magnets magnetized in the axial direction. One of the magnets, the inner PM, is set based on the rotor-impeller circumference. The other, the outer PM, is fixed based on the inner surface of the casing. The rotor-impeller has its top yoke part on the top stator side and its bottom yoke part on the bottom stator side. A closed type impeller with six vanes was constructed between the top yoke part and the bottom yoke part of the rotor-impeller. The diameter and thickness of the rotor-impeller are 60 mm and 20 mm, respectively. A pump casing was constructed between the top and the bottom stators, and the rotor-impeller was enclosed in this casing. The axial gap between the rotor-impeller and the top stator is 2 mm. The axial gap between the rotor-impeller and the bottom stator is 2.8 mm. The axial blood gap between the rotor-impeller and the pump casing is 0.5 mm. The radial gap between the rotor-impeller and the pump casing is 1 mm. The

height and diameter of the Maglev pump are 54 mm and 95 mm, respectively. Figure 2 shows a block diagram of control system of the Maglev pump. The rotor levitation and rotation is controlled with a digital PID control algorithm using dSPACE 3.2. Four eddy current sensors are used to measure the rotor position in the axial direction and its tilt angles. A rotary encoder with a hall sensor was set around the circumference of the rotor to measure and control the rotating speed. Control in the axial position and control of the tilt is maintained by adjusting the attractive force acting on the rotor-impeller. The attractive force in the axial direction F_a (N) produced by the position control current I_a (A) in the top stator that acts on the rotor-impeller is as follows:

$$F_a = \frac{2\left(NI_a/R + BS\right)^2}{S\mu_0} \quad \text{.....(1)}$$

Where μ_0 is the permeability of a vacuum, $4\pi \times 10^{-7}$ (H/m). N is the number of turns in the electro-magnetic coil (turns). R is the magnetic resistance of the gap between the top stator and the rotor-impeller (H^{-1}). B is the bias flux density produced by the permanent magnet on the top stator (T). S is the cross-section area of the gap between the top stator and the rotor-impeller (m^2).

Design of the PM bearing

The PM bearing produces a stiffness characteristic in the radial direction. However, an unstable axial repulsive force is generated when the inner PM on the levitated rotor shifts axially towards the outer PM. Therefore, instability in the axial direction increases with an increase in the radial stiffness of the PM bearing, creating a trade-off problem. The radial PM bearing should be designed from the point of view of balancing the axial active bearing. Also, the energy consumption and the size of the device are limited in terms of being an implantable artificial heart. We must consider both a lower input power and a smaller size of the active magnetic bearing simultaneously.

Numerical simulation of the repulsive force: A numerical simulation based on surface current density theory [5] was developed and performed to estimate the repulsive force produced by the PM bearing. Equation 2 describes the surface current density theory used in the numerical simulation. ΔF denotes the repulsive force for the small elements, ΔR and $\Delta R'$ of the inner PM and outer PM, respectively. ΔF, ΔR, and $\Delta R'$ are three dimensional vectors:

$$\Delta F = \frac{M^2}{4\pi\mu_0} \frac{\Delta R - \Delta R'}{\left|\Delta R - \Delta R'\right|^3} \quad \text{.....(2)}$$

Where M is the magnetization (Wb/m^2). The repulsive force produced by the PM bearing is

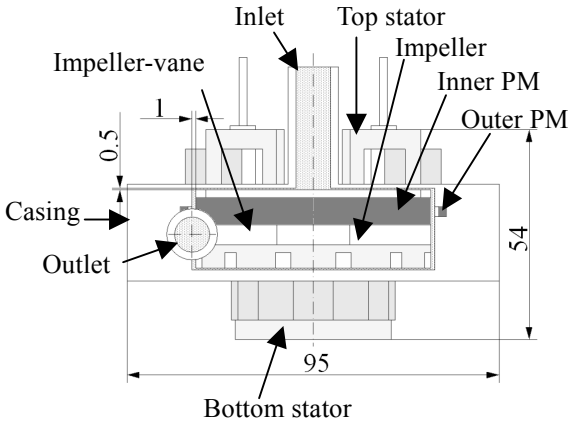

Figure 1: Maglev centrifugal blood pump

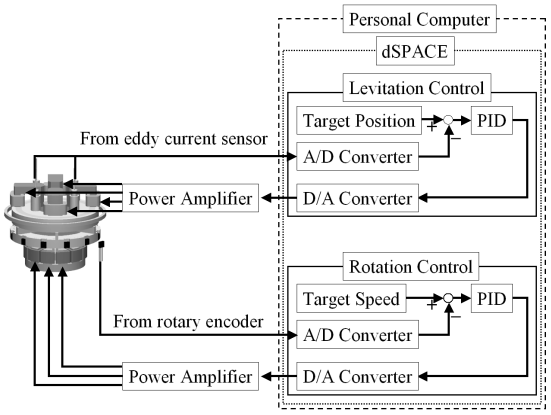

Figure 2: Block diagram of control system

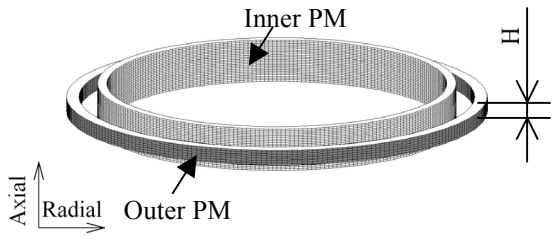

Figure 3: Analysis model of the numerical simulation

calculated by summing ΔF of all elements. Each permanent magnet was modeled by dividing the area into 100 parts in the circumferential direction and 50 parts in the axial direction. This analysis model is shown in Figure 3. The height, inner diameter, and outer diameter of the inner PM were fixed at 7 mm, 55 mm, and 58 mm, respectively. Inner and outer diameters of the outer PM were also fixed at 64 mm and 68 mm, respectively. The height of the outer PM, H, and the axial and radial positions of the inner PM were changed in the simulation. Two types of PM bearings were designed based on the simulation results. One of the PM bearings is referred to as the low stiffness type, the other as the high stiffness type.

Evaluation of the suspension force: The control performance in the axial direction of the active magnetic bearing was evaluated to determine the spring rate of the PM bearings. The attractive force in the axial direction produced by the top and bottom stators was measured directly with a force gauge sensor. The repulsive force in the radial direction was also measured directly with the force gauge sensor to evaluate suspension performance in the radial direction for both types of PM bearings.

EXPERIMENTS

The impulse response was measured to confirm levitation stability. The rotor-impeller was levitated without rotation and was hammered in the radial and axial directions. The levitation performance was evaluated in air. The Maglev centrifugal pump was connected to a closed mock circuit filled with water, and levitation performance was evaluated.

RESULTS

Design of the PM bearing

Numerical simulation of the repulsive force: The spring rate of the PM bearing was estimated by dividing the calculated repulsive force by the displacement of the inner PM. Figure 4 shows the relationship between the estimated spring rate of the PM bearing and the height of the outer PM. In the numerical simulation, the estimated spring rate in the radial and axial directions changed in proportion to the height of the outer PM, and the spring rate in the axial direction was twice as strong as that in the radial direction.

Evaluation of the suspension force: The top stator could produce an attraction of 32 N over the 2 mm air gap between the rotor-impeller and the top stator. The bottom stator could produce an attraction of 12 N over the 2.8 mm air gap between the rotor-impeller and the top stator. The controllable displacement of the rotor-impeller was plus or minus 0.5 mm in the axial direction. The height of the low and high stiffness types were determined to be 2.5 mm (Estimated spring rate 2.5 N/mm) and 3.5 mm (Estimated spring rate 3.5 N/mm) based on the results of the numerical simulation and the evaluation of the control performance in the axial direction of the active

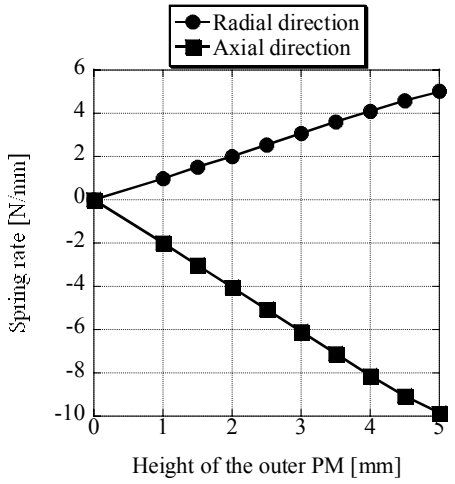

Figure 4: Estimated spring rate of the PM bearing

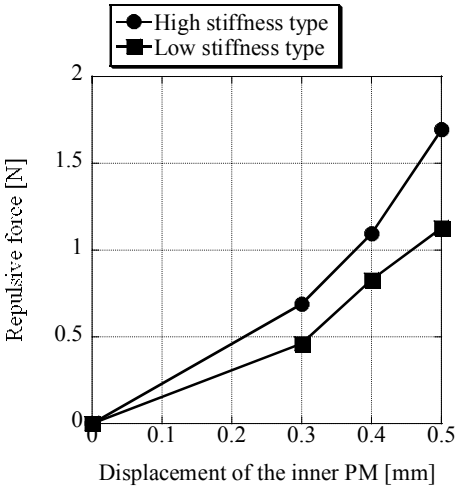

Figure 5: Measured repulsive force

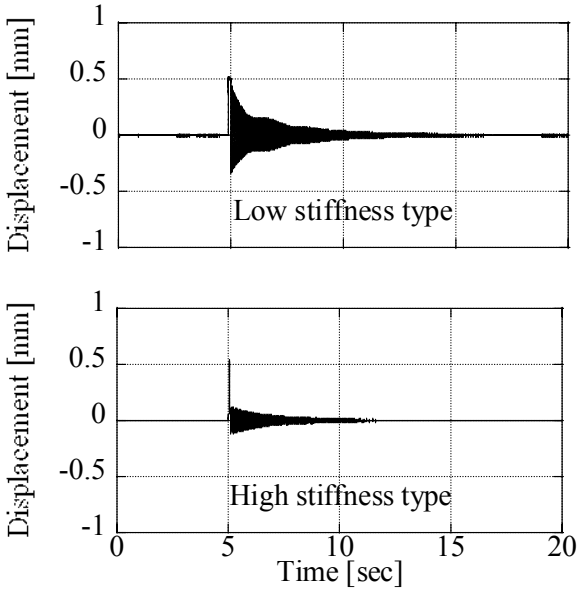

Figure 6: Impulse response in radial direction of the rotor-impeller

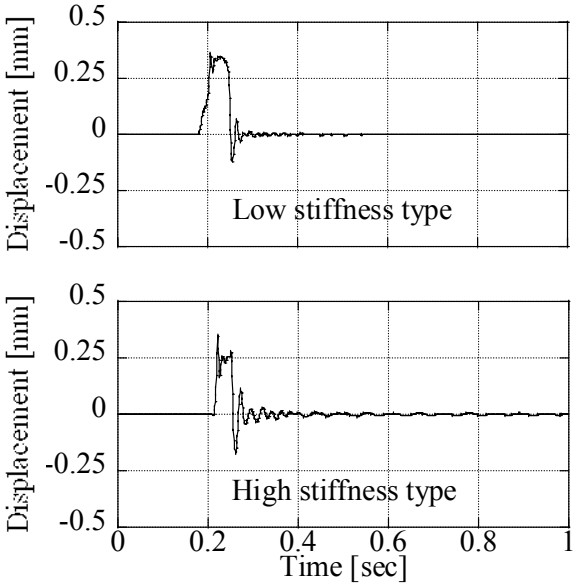

Figure 7: Impulse response in the axial direction of the rotor-impeller

magnetic bearing. Figure 5 shows the measured repulsive forces produced by the PM bearings. When the inner PM moved 0.5 mm in the radial direction, the repulsive force produced by the low and high stiffness type PM Bearing were 1.2 N and 1.7 N, respectively. The spring rates of the low and high stiffness type PM bearings are 2.4 N/mm and 3.4 N/mm, respectively. The spring rates of the low and high stiffness type PM bearings were nearly the same as those calculated by the numerical simulation.

Impulse response

The impulse responses in the radial and axial directions of the Maglev pump with the low and high stiffness type PM bearings are shown in Figure 6 and Figure 7, respectively. The transient response in the radial direction of the low and high stiffness types decayed for 10 sec and 7 sec, respectively. The transient response in the axial direction of the low and high stiffness types decayed for 0.15 sec and 0.2 sec, respectively.

Levitation performance in air

The maximum oscillating amplitude in the axial and radial directions is shown in Figure 8 and Figure 9, respectively. The maximum rotational speed of both the low and high stiffness types was 3000 rpm. The maximum oscillating amplitude in the axial direction, controlled actively by the stator in both stiffness types, was 0.19 mm. The rotor-impeller of the low stiffness type touched the casing at a rotation speed of 1000 rpm and 1400 rpm. The rotor-impeller of the high stiffness type touched the casing at a rotation speed of 1200 rpm only. Figure 10 shows the levitation power consumption of the low and high stiffness types. At a rotation speed of 1500 rpm, the power consumption for levitation in the low and high stiffness types was 1.2 W and 1.7 W, respectively.

Levitation performance in water

Figure 11 and Figure 12 show the change in oscillation amplitude in the axial and radial directions of the levitated rotor during pumping due to increasing rotation speed. Figure 13 shows the HQ characteristics of the Maglev pump. The maximum rotational speed, the maximum flow rate, and the maximum head pressure for both types were 2000 rpm, 10 l/min, and 200 mmHg, respectively. The maximum oscillating amplitude in the axial direction, controlled actively by the stator in both stiffness types, was 0.05 mm. The maximum oscillating amplitudes in the radial direction of the low and high stiffness

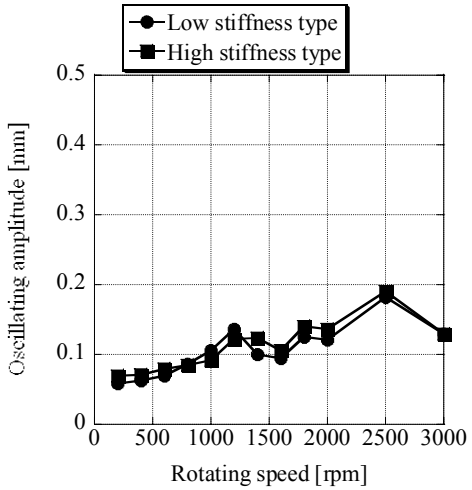

Figure 8: Maximum oscillating amplitude in the axial direction in air

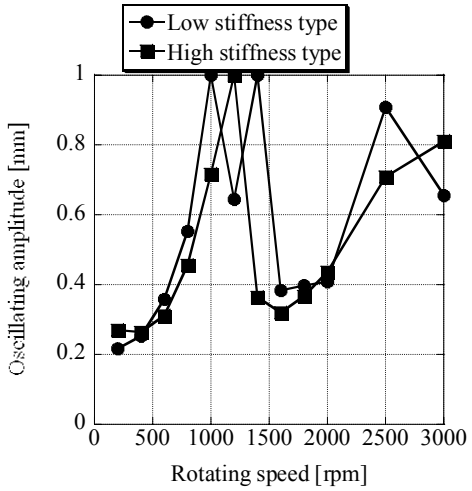

Figure 9: Maximum oscillating amplitude in the radial direction in air

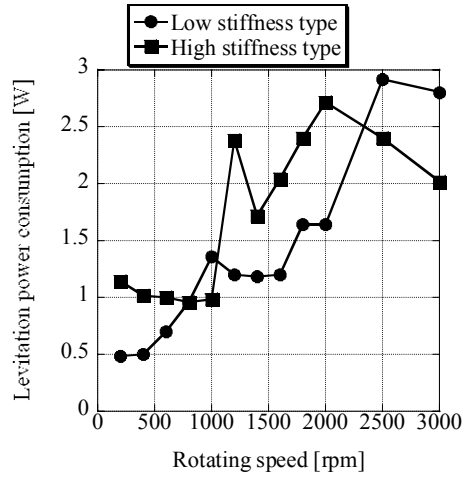

Figure 10: Power consumption of the Maglev pump with the low and high stiffness type in air

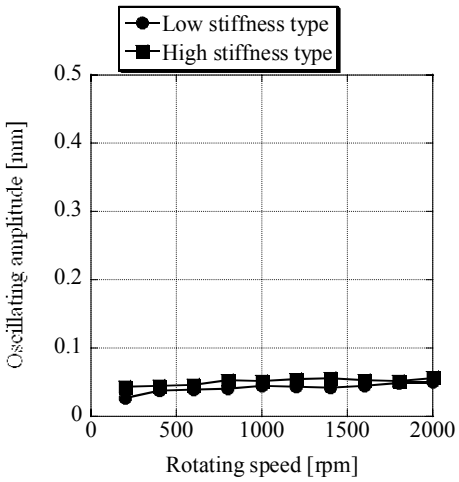

Figure 11: Maximum oscillating amplitude in the axial direction in water

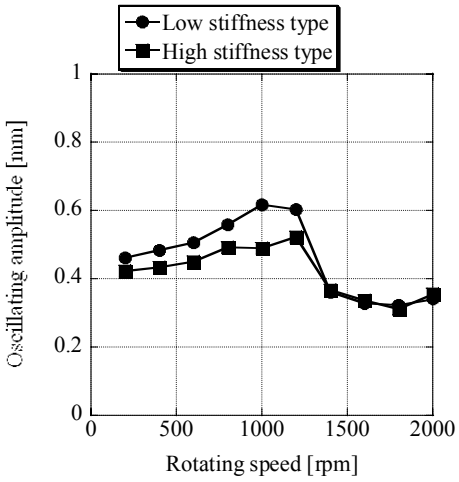

Figure 12: Maximum oscillating amplitude in the radial direction in water

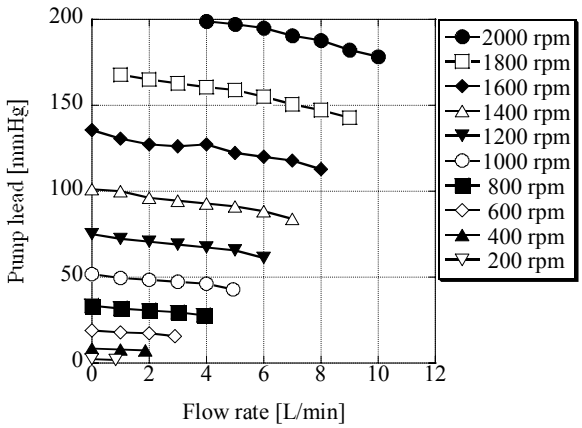

Figure 13: HQ characteristics

types were 0.5 mm and 0.6 mm, respectively. A pressure head of 100 mmHg and a flow rate of 5 l/min were generated with at a rotation speed of 1500 rpm. The maximum oscillating amplitude in the radial direction for both types and the total power consumption including motor power at this point was 0.3 mm and about 10 W, respectively.

DISCUSSION

The numerical simulation of the repulsive force showed that the spring rate in the axial direction is twice as strong as that in the radial direction. This result suggests the following relationship. If the spring rate in the radial direction is too high, stability in the axial direction will decrease, resulting in an increase in the power consumption for levitation. In the experimental results for the impulse response and levitation performance in air and water, the difference in stability due to a difference in the stiffness of the PM bearing was confirmed. Although the stability in the radial direction of the high stiffness type is superior to that of the low stiffness type, the stability in the axial direction of the high stiffness type was lower. A Maglev pump that used the high stiffness PM bearing would have poor control in the axial direction. Additionally, at rotation speeds near 1500 rpm, the power consumption for levitation of the high stiffness type was 40 % higher compared with that of the low stiffness type. In the levitation experiment in air, the rotor-impeller collision with the casing in the radial direction was the effect of the resonance frequency of the magnetic suspension in the radial direction. However, in the levitation experiment in water, the oscillating amplitude in the radial and axial directions decreased due to the damping effect of water, preventing any collisions. The pump developed here displayed particularly good magnetic suspension performance in the axial direction. Since the low stiffness type has sufficient magnetic support performance, although the stability in the radial direction is low compared with the high stiffness type, and total power consumption is low, the low stiffness type seem to be the better. The overall pump performance of the developed Maglev pump is good enough for use as a left ventricular assist system.

CONCLUSION

The PM bearing was designed based on a numerical simulation. The PM bearing restricted the radial movement of the levitated impeller without deterioration of the axial position control performance. This Maglev centrifugal pump displayed sufficient pump performance for use as a ventricular assist device. In the future, improvement in restricting the radial movements of the rotor-impeller and miniaturization of this Maglev pump will be explored.

ACKNOWLEDGEMENT

This work was supported financially, in part, by a Grant-in-Aid for Scientific Research (B) from Japan Society for the Promotion of Science (no.14380389).

REFERENCE

1. Schoeb R, Barletta N, Fleischli A, Foiera G, Gempp T, Reiter H-G, Poirier VL, Gernes DB, Bourque K, Loree HM, Richardson JS, A bearingless motor for a left ventricular assist device (LVAD), 7th ISMB August 23-25, (2000), 383-388.
2. Nojiri C, Kijima T, Maekawa J, Horiuchi K, Kido T, Sugiyama T, Mori T, Sugiura N, Asada T, Shimane H, Nishimura K, Ban T, Akamatsu T, Ozaki T, Ito H, Suzuki M, Akutsu T, More than 1 year continuous operation of a centrifugal pump with a magnetically suspended impeller, ASAIO Journal, 43-5 (1997), 548-552.
3. Allaire P, Hilton E, Baloh M, Maslen E, Bearson G, Noh D, Khanwilkar P, Olsen D, Performance of a continuous flow ventricular assist device: magnetic bearing design, construction, and testing, Artificial Organs, 22-6 (1998), 475-480.
4. Masuzawa T, Onuma H, Kim SJ, Okada Y, Magnetically suspended centrifugal blood pump with a self-bearing motor, ASAIO Journal, 48 (2002), 437-442.
5. Tsui J, Iden D, Strnat K, Evers A, The Effect of Intrinsic Magnetic Properties on Permanent Magnet Repulsion, IEEE Transactions on Magnetics, Vol.Mag-8, No.2, June 1972: 188-194